To appear in the *Journal of Hydraulic Research*
Vol. 00, No. 00, Month 20XX, 1–24

Research paper

An experimental study on violent geysers in vertical pipes

ARTURO S. LEON (IAHR Member), Associate Professor, *Department of Civil and Environmental Engineering, University of Houston, Houston, Texas, United States*
Email: aleon3@uh.edu (author for correspondence)

IBRAHEM S. ELAYEB, Former Graduate Student, *School of Civil and Construction Engineering, Oregon State University, Corvallis, Oregon, United States*
Email: elayebi@onid.oregonstate.edu

YUN TANG, Graduate Student, *Department of Civil and Environmental Engineering, University of California at Davis, Davis, California, United States*
Email: yuntang@ucdavis.edu

An experimental study on violent geysers in vertical pipes

ABSTRACT

This paper reports a laboratory study on violent geysers in a vertical pipe. Each geyser produced consists of a few consecutive violent eruptions within a time frame of a few seconds with heights that may exceed 30 m. Herein, the term "violent" is used to distinguish the present work from previous studies, which reported geyser heights that were relatively small compared to the present study. Previous work has speculated that the extreme behavior of geysers is driven by the buoyant rise of the air pocket in the vertical pipe. The present study shows that once the air pocket breaks through the free surface and produces a water spill, the horizontal pipe flow dynamics, in particular the rapidly changing pressure gradient following the first weak eruption, is driving the entire geyser mechanism.

Keywords: Combined sewer overflows; combined sewer system; experiment; geyser; stormwater; transient; violent eruption

1 Introduction

Although combined sewer overflow (CSO) storage tunnels are unique in their geometry, in general, these systems consist of near-horizontal pipes or tunnels, which serve as storage, and vertical shafts, which serve as ventilation columns or as access points for maintenance. During intense rainfall events, CSO storage tunnels may undergo a rapid filling, leading to highly dynamic conditions and air entrapment (e.g., Hamam & McCorquodale, 1982; Vasconcelos, 2005; Leon, Ghidaoui, Schmidt, & García, 2010; Lewis, 2011; Wright, Lewis, & Vasconcelos, 2011). When the entrapped air arrives at a vertical shaft (dropshaft), a high frequency oscillatory release (e.g., eruption) of a mixture of gas (e.g., air) and liquid may occur. The oscillating jet of gas-liquid mixture may reach a height of the order of a few to tens of meters above ground level. Most geyser videos available in the web present multiple independent geyser events (e.g., `http://www.youtube.com/watch?v=4aQySLOsKys`), each of which consists of several eruptions. Each independent geyser is very likely associated to a different isolated air pocket. Wright et al. (2011) reported nine independent geysers in a stormwater collection system in Minneapolis, each of which consisted of several eruptions, and each geyser lasted for about 10-25 s with about 75-90 s separating the onset of each geyser.

Violent geysers may be destructive. A video of a geyser that occurred at Interstate 35W (Minnesota) on 07/03/1999 can be seen at `http://www.youtube.com/watch?v=4aQySLOsKys` (Minnesota-DOT, 1999). To avoid geysering and their associated consequences, combined sewer systems (CSSs) often are not operated at their full capacity (e.g., Leon, 2016b). Not operating CSSs at their full capacity means that these systems are not fully utilized and hence, combined sewer overflows (CSOs) occur more often than they should. The U.S. Environmental Protection Agency (EPA) estimates that in 31 states and the District of Columbia, 772 combined sewer systems with more than 9,000 CSO outfalls discharge about 3.2 billion cubic meters (850 billion US gallons) of untreated wastewater and stormwater annually (EPA, 2004). Combined sewer overflows contain not only stormwater but also untreated human and industrial waste, toxic materials, and debris, which have a negative impact on water quality and recreational uses in local waterways.

Geysers have been studied over three decades in terms of water phase only or air-water interaction (e.g., Guo & Song, 1991; Lewis, 2011; Wright et al., 2011; Shao, 2013). These studies include laboratory experiments and numerical modeling. Several of these studies focused on the analysis of dynamic flow conditions under which surges and geysers could occur. Hamam and McCorquodale (1982), Vasconcelos (2005) and Lewis (2011) studied the mechanisms through which air is entrapped in horizontal tunnels. Furthermore, a number of laboratory experiments (e.g., Vasconcelos, 2005; Lewis, 2011) have been conducted to produce geysers, however none of these experiments produced large geyser heights as observed in the field. For instance, in the experiments of Lewis (2011), the maximum geyser height achieved was 2.3 m for a 44 mm vertical pipe and 0.65 m for a 95 mm vertical pipe.

Field studies on geysers are rarely documented due to their seldom occurrence. A series of geysers at a tunnel system below Interstate 35W (Minnesota) were documented, however the sampling rate of the data was inadequate for a detailed analysis (Wright et al., 2011). Wright et al. (2011) pointed out that the maximum pressure head recorded was far below the pressure required to lift the water to the ground level. Also, pressure data indicated no inertial oscillations. These authors concluded that "geyser formation in this tunnel system is not directly connected with surging in the tunnel system".

In general, previous work has speculated that geysers are driven by the buoyant rise of air pockets in a vertical pipe. The present work shows that once the air pocket breaks through the free surface and produces a water spill, the horizontal pipe flow dynamics drives the entire geyser mechanism. The present work has produced violent geysers in a laboratory setting that resemble those observed in actual stormwater and combined sewer systems (e.g., a few consecutive violent eruptions within a time frame of a few seconds with heights that may exceed 30 m). As an example, Fig. 1 shows three snapshots of a geyser produced in one of our laboratory experiments with a vertical pipe length of 6 m. It can be noticed in Fig. 1 that the geyser produced is not simply a splash of air and water but a violent eruption of a mixture of air and water, which resembles the characteristics of actual geysers as documented in recorded videos available in the web (e.g., `http://www.youtube.com/watch?v=4aQySL0sKys`). In a similar way to the Minnesota geyser video, the first eruption of the laboratory geysers was not the strongest in terms of intensity (e.g., height). Also, in a similar way to the Minnesota events, each laboratory geyser consisted of few violent eruptions with large eruption heights. Under the geyser definition of Wright et al. (2011), whose authors define a geyser as a set of a few consecutive eruptions, only a single geyser event (i.e., few consecutive eruptions) was produced in each of the present laboratory experiments.

To demonstrate that geysers can be minimized by decreasing the air mass flow rate entering the vertical pipe, the second part of the experiments considered an orifice device at the bottom of the vertical pipe. It is clear that an orifice would not be a practical retrofitting method as it would constitute an impediment to stormwater flow admissions, reduction of air ventilation during a filling event and an obstruction for maintenance. This paper is divided as follows. First, the experimental setup, the measurement equipment and experimental procedure are presented. Second, the experimental results including the dimensional analysis and the mechanisms leading to geysers are presented and discussed. Finally, the key results are summarized in the conclusion.

2 Experimental work

2.1 *Experimental Setup*

The apparatus for the experimental study is shown schematically in Fig. 2. The horizontal and vertical pipe consisted of clear PVC schedule 40 with an internal diameter of 152.4 mm (6″). The upstream tank, which was made of fiberglass, has a total volume of 1.7 m^3 (450 US gallons) and a maximum operating absolute pressure head of 105.5 m (150 psi). It is worth mentioning that the ratio of initial volume of air to initial volume of water in the present experiments ranged from 4.5 to 7.8, which ratios are much larger than previous experimental investigations on geysers. The upstream tank is connected to the horizontal pipe through a 152.4 mm gate valve, which controls the flow from the head tank. Another ball valve with 76.2 mm (3″) diameter was installed at the end of the downstream pipe to drain the water from the system. The experimental setup was installed outdoors in an open-air environment. It was noticed in our early preliminary experiments that when the wind was relatively strong, the geyser plume would be significantly shifted with respect to the axis of the vertical pipe. To diminish the wind effects, the experiments were performed only when the wind was light for which there was not apparent shift of the geyser plume.

Eight experimental configurations were created by varying three parameters. The first parameter was the vertical pipe length (3, 6, 9 and 12 m), which is the same as the initial water depth in the vertical pipe. The second parameter was the initial water volume in the tank, which were

0.7760 m^3 (205 US gallons) and 0.9615 m^3 (254 US gallons). The third parameter was the initial air absolute pressure head in the upstream tank, which values are shown in Table 1 and were obtained by iteration as described in the *Experimental procedure* subsection. Every experimental run was repeated fifteen times, which resulted in a total of 120 experiments. The geyser heights are consistent as shown by the relatively small coefficient of variations (e.g., ratio of the standard deviation to the mean) presented in Table 2.

The second part of the experiments considered an orifice device at the bottom of the vertical pipe (Fig. 3). Three orifice diameters were tested, namely 76.2 mm ($d/D = 1/2$), 38.1 mm ($d/D = 1/4$) and 19.1 mm ($d/D = 1/8$), where D is the vertical pipe diameter and d is the orifice diameter. In a similar way to the geyser experiments with no orifice, eight experimental configurations were created for each orifice diameter by varying the same three parameters (vertical pipe length, initial water volume and initial air pressure in the upstream tank). Every experimental run was repeated at least nine times, which resulted in at least 72 experiments for each orifice. The total number of orifice experiments performed were 252.

The data collected in the experiments included water temperature (T_w), air temperature (T_a), pressure heads at various locations inside the horizontal and vertical pipe, and the maximum geyser height, which is measured from the top of the vertical pipe. The maximum geyser height is determined from the video recordings using a known reference length located in the vertical pipe (i.e., distance from top of vertical pipe to pressure transducer located 0.76 m below it), which is in the same depth plane as the geyser eruption. For minimizing perspective error (also known as parallax) while maintaining good visibility of the eruptions, the Edgertronic camera was located as far away as possible from the vertical pipe in order to increase the depth of field. Depending on the eruption height and vertical pipe length, the camera was located between 50 and 200 meters away from the vertical pipe. The eruption height was calculated using the MATLAB image processing toolbox by utilizing the pixel dimension of the reference length. The geyser velocity at the top of the vertical pipe was not directly measured in the experiments. There was an attempt to measure the velocity using the video recordings, however the plume of any geyser eruption was highly affected by the plume of the preceding and/or following eruption, which did not allow the tracking of a single eruption.

2.2 *Visualization experiments*

Due to the limited number of pressure transducers available for the experiments (9), the pressure transducers were located depending on the focus of the experiments (visualization or non-visualization). The visualization experiments (50 repetitions) were performed for conditions without orifice only while as the non-visualization experiments were performed for conditions with and without orifice. The non-visualization experiments utilized the array of pressure sensors shown in Fig. 2 while as the visualization experiments used the array shown in Fig. 4. The objective of the visualization experiments was to study the flow patterns in the horizontal pipe and thus, the need to include more pressure sensors in the horizontal pipe. The visualization experiments were performed for a vertical pipe length of 6 meters only. To differentiate the identification of pressure transducers between the visualization and non-visualization experiments, all figures of pressure heads are specifically labeled as either visualization or non-visualization experiments. It is noted in Fig. 4 that two pressure transducers were used at each cross-section in the horizontal pipe. The exact location for the transducer labeled at the top (e.g., P6) was the crown of the pipe while as the location for the transducer labeled at the bottom (e.g., P7) was 12.7 mm above the pipe invert as shown in Fig. 4. In general, the signals produced by pressure transducers located at the same cross-section are almost identical.

2.3 *Measurement equipment*

The measurement equipment used in this study includes:

(1) Nine piezo-resistive pressure transducers (UNIK 5000) (absolute pressure range from 2.5 to 63.3 m H_2O, frequency response of 3.5 KHz, and accuracy of 0.04% full-scale).
(2) Two high-speed video cameras (Edgertronic) [All experiments were recorded at 120 frames per second].
(3) Two National Instruments data acquisition board NI 6321 with eight differential channels and sampling rate up to 250 kHz integrated with LabVIEW.
(4) Two thermometers (measurement range from -3 to 40 °C with an accuracy of 0.2 °C), which were used to measure water and air temperature at the beginning of each experiment.

2.4 *Experimental procedure*

The experimental procedure was as follows:

(1) Keeping the steel gate valve fully closed, the upstream tank is partially filled with water (0.7760 m^3 or 0.9615 m^3).
(2) The upstream tank is pressurized with air to a pre-specified pressure and the data acquisition system (DAQ) started to acquire data. The pre-specified pressure was obtained by iteration in such a way that (1) the steel gate valve can be fully opened slowly ($\approx$ 20-50 seconds) without releasing air from the tank, and (2) after the gate valve is fully opened, the water level in the tank is at its bottom (i.e., air has occupied the entire tank). The latter condition is necessary to produce a geyser. If after opening the valve, the water level in the tank was significantly above its bottom (e.g., more than about 10 mm), geysering did not occur as the air in the tank was never admitted into the horizontal pipe. It is noted that even though the duration of the valve opening has some variability, it does not play a significant role on the geysering as after the valve is fully opened, the system is in apparent equilibrium where the pressure heads recorded by all transducers in the horizontal pipe and air tank are the same (e.g., see pressure heads between 60 and 74 seconds in Fig. 5) and are equal to the hydrostatic pressure head due to the water column in the vertical pipe.
(3) Once the gate valve is fully opened and the water level is at the bottom of the tank, the system is in apparent equilibrium. This is the case for both initial water volumes and hence, both water volumes resulted essentially in the same geyser intensity. Thus, no distinction is made between both water volumes. Shortly after the aforementioned apparent equilibrium, the air-water interface at the bottom of the air tank oscillates up and down slightly which quickly grows and then leads to the air admission from the air tank to the horizontal pipe. The geyser eruptions would occur shortly after the air admission, which would occur between ten seconds to one minute after the gate valve is fully opened. Figure 5 shows an example of the complete time trace of pressure heads recorded for a vertical pipe length of 6 m. In this figure, the horizontal pipe downstream of the gate and the dropshaft are initially dry. At about 17 seconds, the gate opening is started and the gate is completely opened at about 60 seconds. As can be seen in Fig. 5, the sensors downstream of the gate and those in the dropshaft started to get submerged with water at a time between 29 and 38 seconds. Between 40 and 52 seconds there was significant water spill on top of the dropshaft. At about 55 seconds, the water spill at the top of the dropshaft ceased almost completely. At this time (55 s), the water level in the tank was at its bottom and air has not entered yet to the horizontal pipe. Between 60 and 74 seconds, the system is in apparent equilibrium as observed by the constant pressure heads in the tank (transducer P1) and the horizontal pipe (transducers P2 and P3), which pressure heads are equal to the vertical pipe length. During the first few seconds of this time interval (60-74 s), the air-water interface at the bottom of the air tank oscillates up and down slightly

which quickly grows and then leads to the air admission from the air tank to the horizontal pipe. At about 70 seconds, the air in the tank started to be admitted continuously into the horizontal pipe and the geyser eruptions occurred between 76.5 and 82 seconds.

(4) After the eruptions, the system is depressurized and the data recording is stopped. It is worth mentioning that in all geyser experiments, after the geysering is terminated, the water depth at rest in the horizontal pipe was between 10% to 50% of the pipe diameter, which indicates that a large portion of the water (all of vertical pipe and a significant part of horizontal pipe) is lost in the geysering. The large amount of water lost in the geysering allowed the evacuation of all air in the tank.

3 Results and Discussion

3.1 *Mechanisms leading to geysers*

This section briefly describes the mechanisms leading to geysers as observed in the visualization experiments. For an in-depth analysis of the geyser mechanisms including a mathematical model for estimating the maximum velocity of geyser eruption, the reader is referred to Leon (2017). The schematics for our theory on geyser mechanisms is presented in Fig.9, which summarizes the geyser processes in six parts (Figs. 9a-9f.), each of which are briefly described in the caption of the sub-figures. For supplementing the theory, video snapshots for the horizontal pipe are presented in Fig. 7. As mentioned earlier, videos for the horizontal pipe were recorded only for the visualization experiments. For supplementing the explanation, pressure head data (Fig. 6) was also recorded for the visualization experiments. The video snapshots in Fig. 7 correspond to the pressure heads shown in Fig. 6. For maximizing the view of the pressure heads, Fig. 6 does not show the complete time trace of the experiment, however this figure shows part of the *steady state* period right before the air in the tank starts to be admitted into the horizontal pipe to produce the geyser. The main mechanisms that lead to geysering are summarized next:

(1) A large air pocket approaches the vertical pipe causing a small water spill at the top of the vertical pipe (Fig. 9a and 7.1 [$t = 110.086$ s]). Note in Fig. 6 that the air pocket arrived at the location of sensor 2 (Fig. 4) at around 113.6 s. It can be noticed in this figure (transducers P2-P7) that during few seconds, until about 118 seconds, the large air pocket moves slowly in the horizontal pipe without producing significant fluctuations. This can be corroborated with Figs. 7.1 ($t = 110.086$ s)-7.5 ($t = 117.961$ s) that don't show violent flows. The movement of the air pocket in the horizontal pipe is relatively slow because there is no initial significant pressure gradient between the horizontal and vertical pipe. This can be confirmed by the pressure heads of sensors 4-7 (horizontal pipe) between 113.6 and 118 s in Fig. 6.

(2) The large air pocket enters the vertical pipe and rises due to buoyancy causing more water spill at the top of the vertical pipe. Note in Fig. 6 that the pressure sensors in the vertical pipe (transducers P8 and P9) start to show pressure fluctuations shortly after those of pressure sensor 2. The front of the air pocket, which resembles the classical Taylor bubble, occupies almost the entire cross-sectional area of the vertical pipe. The tail of the air pocket ascending in the vertical pipe is highly turbulent with a near homogenous mixture of air and water with great content of void fraction. In a similar way to the classical Taylor bubble, as the air pocket ascends, a significant amount of liquid that is on top of the air pocket is carried upwards and a portion of the water falls on the sides of the pocket (e.g., film flow). This can be observed in Fig. 9b.

(3) When the Taylor-like bubble reaches the top of the vertical pipe, most of the water that is on top of the air pocket is spilled (Fig. 9c).

(4) As water is quickly lost due to spilling, the hydrostatic pressure in the vertical pipe is rapidly reduced, creating a significant pressure gradient between the horizontal and vertical pipe,

which accelerates the air in the horizontal pipe. This rapid acceleration propagates to the vertical pipe and leads to an eruption of a height which is not the largest (Fig. 9d). Subsequently, the rapid increase in air velocity in the horizontal pipe results in the Kelvin-Helmholtz instability that transforms the initial stratified flow regime to wavy (Figs. 7.5 [t = 117.961 s] - 7.7 [t = 118.151 s]) and, eventually, slug flow (e.g., Figs. 7.8 [t = 118.236 s], 7.9 [t = 118.311 s]). A slug flow is a series of liquid plugs (slugs with some entrained air) separated by relatively large air pockets (e.g., Elperin & Fominykh, 1996). It is worth mentioning that even though the vertical pipe is initially filled with water, the geyser will not be produced until part of the water in the vertical pipe is spilled. As can be observed in Fig. 6, the pressure head in the horizontal pipe upstream of the vertical pipe (sensors 2 and 3 in Fig. 4) varied between 1 and 5 meters during the geysering (between 118 and 122 s), which is below the six meters initial water depth in the vertical pipe. The geyser eruptions are distinguished as E1, E2, E3 and so on in Fig. 6. These eruptions are evidenced by a sudden depressurization of pressure transducer P9 (e.g., large flow velocity), which is located near the top of the pipe.

(5) Once the slugs are formed in the horizontal pipe, there is a flow discontinuity and the continuous supply of air from the horizontal to the vertical pipe is blocked. Starting with the slug closest to the vertical pipe, in consecutive order and one at a time, the slugs are violently propelled into the vertical pipe right after each sudden drop of pressure in the vertical pipe (e.g., after a significant pressure gradient between the slug and the vertical pipe). During this process, new slugs can be formed in the horizontal pipe and violently propelled as well. Note in Fig. 6, between 118 and 122 seconds, that geyser eruptions (e.g., large pressure fluctuations at transducer P9) are preceded by large pressure gradients between the horizontal pipe (e.g., transducers P4 and P6) and the vertical pipe (e.g., transducer P8). It can be noticed in Fig. 6 that the pressure head at transducer P2 decays slowly and it is not significantly affected by the pressure head oscillations at transducer P8. This is because of the air flow discontinuity produced by the slugs. The slow decay of pressure head in the horizontal pipe, due to the slugs, provides the pressure to still achieve significant pressure gradients (between the horizontal and vertical pipe) after the first geyser eruption.

It can be noticed in Fig. 6 that the pressures located downstream of the vertical pipe (transducers P6 and P7) have significant fluctuations around the mean pressure. According to the so-called Joukowsky equation, a pressure surge occurs when a fluid in motion is forced to stop or change velocity suddenly. In the geyser experiments, the flow velocity at the downstream end of the pipe is zero (e.g., dead end). However, the flow velocity in the horizontal pipe, upstream of the vertical pipe, may be very high as a result of the eruptions in the vertical pipe. Thus, there is a significant change of velocity in the downstream horizontal pipe (from large velocity at the vertical pipe to zero at the downstream end), which would lead to a significant pressure surge. Note in Fig. 6 that the pressure trace at transducer P8 follows a similar pressure oscillation pattern to that of transducer P6, although with a slight delay. This means that pressure transients in the horizontal pipe have an impact on geyser eruptions as they lead to large pressure gradients between the horizontal and the vertical pipe. It is worth mentioning that the liquid slugs supply the water for the eruptions. Overall, the second or third geyser has the largest intensity in terms of height (Fig. 9e).

(6) After the second or third eruption, there may be a few more eruptions. However, as water is depleted in the vertical pipe and the horizontal pipe is depressurized, the geysering process is terminated. On average, between 3 to 8 eruptions in a time frame of 2 to 10 seconds has been observed. After the eruptions are terminated, the water depth at rest in the horizontal pipe is between 10% to 50% of the pipe diameter (see Fig. 9f and 7.12 [t = 148.586 s]).

3.2 *Geyser dimensional analysis*

The geyser height (h_g) [m] is dominated by the physical constants of the liquid (e.g., water) and gas (e.g., air), namely, the kinematic viscosity (ν) [m^2/s], the density (ρ) [kg/m^3] and the surface tension (σ) [N/m]. The first two variables should be considered for the liquid and gas phases, however as indicated by Pfister and Chanson (2014), the gas constants are of minor significance. In addition, the geyser height is influenced by the gravitational acceleration (g) [m/s^2], the diameter of the vertical pipe (D) [m], the diameter of the horizontal pipe (D_t) [m], the volume and pressure of air entrapped in the horizontal pipe, the vertical pipe length (H) [m] and the initial water depth in the vertical pipe (y_o) [m].

As shown in Eq. (1), the volume and pressure of air entrapped in the horizontal pipe can be agglomerated by the gas mass flow rate ($\dot{M}$) [kg/s]. The expression for the average gas mass flow rate ($\dot{M}$) can be obtained from the ideal gas law and be written as:

$$\dot{M} = \frac{\Delta M}{\Delta t} = \frac{\Delta(P_a V_a)}{R T_a \Delta t} \tag{1}$$

where M is the air mass, P_a is the air pressure in Pascals, V_a is air volume in m^3, T_a is the air absolute temperature in Kelvin (K), R is the individual gas constant in $J/(kgK)$ and Δt is the duration of the geysering event, which is defined as the period from the entry of the air pocket to dropshaft until the ending of eruptions. The constant R for air is 287.058 $J/(kgK)$. The duration of the geysering event Δt was obtained from the measured pressure traces by identifying the beginning and ending of pressure fluctuations. It is clear that due to the highly unsteady nature of the geysers, the air mass flow rate leaving the vertical pipe is not constant, however as shown later, the average mass flow rate can be a good indicator for estimating geyser height.

Thus, the geyser height, in a two-phase air-water flow, is a function of the following variables:

$$h_g = f(H, y_o, g, D, D_t, \dot{M}, \rho_w, \sigma, \nu_w) \tag{2}$$

where the subindex w indicates the water liquid. There are ten variables in Eq. (2) and three basic dimensions (mass, length and time). Thus, seven dimensionless terms can be obtained as shown below:

$$\frac{h_g}{D} = \phi\left(\frac{\dot{M}}{\rho_w\sqrt{gD^5}}, \frac{H}{D}, \frac{(\sqrt{gD})D}{\nu_w}, \frac{\rho_w(\sqrt{gD})^2 D}{\sigma}, \frac{D_t}{D}, \frac{y_o}{D}\right) \tag{3}$$

The third and fourth dimensionless terms on the right side of Eq. (3) are equivalent to the Reynolds number (R) and the Weber number (We), respectively, where the term $\sqrt{gD}$ can be thought as a characteristic velocity. The Weber number, which is a measure of the relative importance of the fluid's inertia compared to its surface tension, in vertical pipes, is defined using as characteristic length either the pipe diameter or the representative bubble diameter (e.g., Sefko & Edin, 2015; Sharaf, der Meulen, Agunlejika, & Azzopardi, 2016). When using the pipe diameter as characteristic length, Sharaf et al. (2016) presents, in Fig. 1 of their publication, the flow patterns in a vertical pipe as a function of the liquid and gas Weber numbers. For the set of experiments of the present paper, the minimum geyser eruption velocity is about 5 m/s (e.g., characteristic velocity), $D = 152.4$ mm, $\nu_w \approx 10^{-6}$ m^2/s, and $\sigma \approx 73 \times 10^{-3}$ N/m. Noting that for bubbly flows, the gas and liquid velocity are similar (e.g., Stefanski, Kalawa, Mirek, & Stepien, 2017), the liquid and gas Weber numbers for the above values are about 52,000 and 64, respectively. By plotting these values in Fig. 1 of Sharaf et al. (2016), the flow pattern corresponds to bubbly flow, which is observed in the vertical pipe during the geysering. Also, literature in the area of two-phase flows suggests that for high-speed air-water flows, scale effects related to air concentration are small when $\mathsf{R} > 3{\times}10^5$ and $\mathsf{We}^{0.5} > 170$ (e.g., Pfister & Chanson, 2014). One may argue that the context of Pfister and Chanson (2014) work is focused in small air bubbles, however after the Taylor-like bubble reaches the top of the vertical pipe and produces the water spill and the subsequent flow acceleration, the flow in the vertical pipe is highly turbulent with a near homogenous mixture of air and water (i.e., small air bubbles). Because air concentration is highly related to geyser occurrence (e.g., air-water mixture), the above limits for R and We may be applicable to geyser flows as well. For the above values, R and $\mathsf{We}^{0.5}$ are 7.5×10^5 and 227, respectively, which are larger than the above limiting values. From the discussion above, the fourth and fifth dimensionless terms can be neglected.

The sixth dimensionless term (D_t/D) has not been explored herein, as the ratio D_t/D has been set to one. However, from the air supply point of view, it is expected that the orifice experiments with $d/D = 1/2$, $1/4$ and $1/8$ are equivalent to those with D_t/D ratios of $1/2$, $1/4$ and $1/8$, respectively. The latter is a speculation and will be explored in a subsequent study. As will be discussed later, the non-orifice experiments and those with an orifice for $d/D = 1/2$ result basically in the same geyser height. The latter means that a horizontal to vertical pipe diameter ratio (D_t/D) larger than $1/2$ likely doesn't influence the geysering. The latter is because there is not significant bottleneck of air supply from the horizontal pipe to the vertical pipe for ratios larger than about $1/2$. As discussed later, geyser intensity is directly proportional to the air mass flow rate. Hence, the conditions tested herein $(D_t/D = 1)$ represent those prone to more intense geysers as air supply may not be a limiting factor. In actual combined sewer systems, even though the ratio D_t/D can be smaller than $1/2$ in early portions (e.g., upstream) of the systems, in most downstream regions, the tunnel diameter often exceeds the dropshaft diameter. The conditions explored in the present study would be applicable only to those downstream regions with unlimited air supply, which according to the present study are associated to most intense geysers. For the latter conditions, the sixth dimensionless term (D_t/D) could be neglected. However, in general, the term D_t/D cannot be neglected. Thus, the relevant dimensionless terms for the geysering can be reduced to:

$$\frac{h_g}{D} = \phi\left(\frac{\dot{M}}{\rho_w\sqrt{gD^5}}, \frac{H}{D}, \frac{y_o}{D}, \frac{D_t}{D}\right) \tag{4}$$

To represent h_g/D as a function of the second, third, fourth and fifth dimensionless terms in Eq. (4), it is assumed that h_g/D obeys the following power form:

$$\frac{h_g}{D} = \alpha 1\left(\frac{\dot{M}}{\rho_w\sqrt{gD^5}}\right)^{\alpha 2}\left(\frac{H}{D}\right)^{\alpha 3}\left(\frac{y_o}{D}\right)^{\alpha 4}\left(\frac{D_t}{D}\right)^{\alpha 5} \tag{5}$$

where $\alpha 1$, $\alpha 2$, $\alpha 3$, $\alpha 4$ and $\alpha 5$ are empirical constants.

The current study is limited to conditions when the initial water depth in the vertical pipe is the same as the drophsaft length $(y_o = H)$ and those where the diameter of the vertical pipe is the same as that of the horizontal pipe $(D_t = D)$. Because of the limited conditions explored in the experiments, only the $\alpha 1$, $\alpha 2$ and $\alpha 3$ coefficients in Eq. (5) are used in the data fitting, which is discussed in the next section. It is pointed out that for conditions where $y_o = H$, most of the geysers start near the top of the vertical pipe which facilitates the measurement of the geyser height using a high-speed video camera. Finally, it is cautioned that the dimensional analysis assumes the physical mechanisms occur similarly to the experiments tested; extrapolating the experimental conditions in any direction significantly from those studied may not lead to the relationships shown in the Data Analysis and Discussion section.

3.3 *Data Analysis and Discussion*

The data collected in the experiments have been analyzed based on the dimensional analysis discussed earlier. To calculate the air mass flow rate, Eq. (1) was used. For estimating $\Delta(P_a V_a)$ in Eq. (1), the initial air pressure is the pre-specified pressure in the tank obtained by iteration (see Table 1). The final pressure is the atmospheric pressure, which is the pressure that is attained immediately after the geyser eruption. The initial air volume is equal to the difference between the volume of the tank and the initial volume of water. The final air volume is equal to the volume of the tank. The volume of the horizontal and vertical pipe are not included in the calculations. The parameter Δt was estimated as explained in the Geyser dimensional analysis section. In practice, the calculation of the air mass flow rate would be difficult. The value of initial $P_a V_a$ could be obtained based on estimates of initial air pressure (e.g., pressure above pipe crown) and initial air volume (e.g., entrapped air volume). The value of final $P_a V_a$ could be set to zero, as it can be assumed that all air volume is released during the geysering. The value of Δt is unknown, however it appears that its order of magnitude is about 10 seconds. Further and more extensive studies are needed to clarify the role of Δt and in general of the air mass flow rate on geysering.

The plot of the dimensionless maximum geyser height as a function of the dimensionless air mass flow rate for the case with no orifice is shown in Fig. 15. As can be observed in Fig. 15, the geyser intensity (e.g., geyser height) increases with the air mass flow rate. According to Leon (2017), there is an upper limit for the geyser velocity (and indirectly for the geyser height), which is given by the sound speed of the air-water mixture in the vertical pipe. This upper limit was obtained by manipulating the equations of conservation of mass, momentum and energy for an accelerating air-water flow in a vertical pipe (Leon, 2017). Figure 15 also shows that the larger is the ratio H/D, the larger is the geyser height. The latter is expected as larger pressure gradients can be achieved for larger H/D ratios.

As mentioned earlier, due to the limited conditions explored in the experiments, only the $\alpha 1$, $\alpha 2$ and $\alpha 3$ coefficients in Eq. (5) are used in the data fitting. The curve fitting along the 80% confidence bounds (if data distribution is approximately normal then 80% of the data values are within 1.28 standard deviations of the mean) are shown in Fig. 16. The coefficients that fit best the data were obtained by the method of non-linear least squares. In the curve fitting, the values of $\alpha 2$ and $\alpha 3$ were 0.511 and 0.667, respectively. Because these values are very close to 1/2 and 2/3, respectively, the values of $\alpha 2$ and $\alpha 3$ were set to 1/2 and 2/3, respectively. Then, a new fitting was performed for $\alpha 1$ while keeping constants $\alpha 2$ and $\alpha 3$. The resulting fitted equation for the dimensionless maximum geyser height is given by:

$$\frac{h_g}{D} = 127.887\left(\frac{\dot{M}}{\rho_w \sqrt{gD^5}}\right)^{1/2}\left(\frac{H}{D}\right)^{2/3} \tag{6}$$

The goodness of fit in Eq. (6) has a R^2 value of 0.92, which indicate a good fit to the data. Figure 16 confirms the good fit of the data for the dimensionless maximum geyser height. It is cautioned that Eq. (6) is limited to the experimental conditions of the present study, which are:

- the horizontal and the vertical pipe diameters were not varied in the experiments. The horizontal pipe diameter used was the same as the vertical pipe diameter ($D_t = D$). As discussed in Section 3.2, this condition would be applicable mostly to downstream regions of combined sewer systems with unlimited air supply.
- a geometry that corresponds to an intermediate vertical pipe linked by two horizontal pipes, which is common but may not be representative of other shaft geometries that experience geysering
- the initial water depth in the dropshaft is the same as the dropshaft length ($y_o = H$).

Because the orifice has a direct influence on the air mass flow rate, it is expected that the geyser height when considering an orifice can still be predicted using the same dimensionless relationship established for the experiments with no orifice. In the curve fitting for the experiments with orifice, the values of $\alpha 2$ and $\alpha 3$ were fixed to the same values as those of the experiments with no orifice. This is justified because very close values to these coefficients are obtained when performing a curve fitting with no fixed coefficients. The curve fitting results for the orifice, no orifice, and combined cases give $\alpha 1$ values of 119.74, 127.89 and 124.96, respectively. The corresponding goodness of fit (R^2) values are 0.89, 0.92 and 0.93, respectively. The latter results show that the values of $\alpha 1$ remain approximately constant and in all cases the R^2 values are equal or higher than 0.89, which indicate a good fit to the data. Figure 17 confirms the good fit of the data for the dimensionless maximum geyser height for the combined case (orifice and no orifice). Figure 17 also shows the respective 80% confidence bounds and the goodness of fit (R^2).

As can be observed in Fig. 17, the geyser heights for orifice A1 (d = 76.2 mm, $d/D = 1/2$) are slightly smaller than those without orifice. This is because the area of the orifice A1 (25% of the cross-sectional area of the vertical pipe) and the cross-sectional area of the initial air flow ($\approx 10 - 30\%$ of the cross-sectional area of the vertical pipe) in the horizontal pipe have similar magnitude and hence there is no much restriction on the air mass flow rate from the horizontal to the vertical pipe. The geyser heights for orifices A2 (d = 38.1 mm, $d/D = 1/4$) and A3 (d = 19.1 mm, $d/D = 1/8$) are much smaller than those without orifice. Figure 17 also shows that the geyser heights for orifice A3 ($d/D = 1/8$) are close to zero. In general, Fig. 17 shows that the larger is the ratio H/D, the larger is the geyser height. Again, the latter is expected as larger pressure gradients can be achieved for larger H/D ratios. Furthermore, the smaller is the orifice diameter, the smaller is the air mass flow rate and the smaller is the geyser height.

Finally, as mentioned earlier, the present experiments were performed using air as the gas. In addition to air, it is argued that in a similar way to lake eruptions (e.g., Zhang & Kling, 2006), geysering in stormwater and combined sewer systems can be enhanced by exsolution of dissolved gases (e.g., Leon, 2016a). The role of exsolution of dissolved gases on the geyser intensity is not part of the present study.

4 Conclusion

This paper presents an experimental study on violent geysers in vertical pipes. The second part of the experiments considered three orifices at the bottom of the vertical pipe. The key results of the present study are as follows:

(1) The present research has produced violent geysers in a laboratory setting with characteristics resembling those geysers that occurred in actual stormwater and combined sewer systems.
(2) The geyser height was found to increase with the dimensionless air mass flow rate.
(3) The geyser height was found to decrease with a decrease of the orifice diameter. In general, the smaller is the orifice diameter, the smaller is the air mass flow rate and the smaller is the geyser height. For the experimental conditions considered in the present study, a geyser eruption is nearly eliminated when the ratio orifice diameter to vertical pipe diameter is about 1/8.
(4) The dimensionless maximum geyser height was found to have a good fit with the relationship obtained in the dimensional analysis.

As discussed in the paper, to facilitate the measurement of the geyser height, the present experiments were focused on a vertical pipe completely full of water, which may not represent field conditions. The role of smaller initial water depths on geyser intensity will be investigated in a subsequent study.

Acknowledgements

The authors are grateful to three JHR anonymous reviewers for their constructive comments, which helped to significantly improve the quality of the manuscript.

Disclosure

This manuscript has not been formally reviewed by EPA. The views expressed are solely those of the authors. EPA does not endorse any products or commercial services mentioned.

Funding

This work was supported by the U.S. Environmental Protection Agency [grant R835187].

Notation

d = orifice diameter (m)
D = diameter of vertical pipe (m)
D_t = diameter of horizontal pipe (m)
g = gravity acceleration ($\mathrm{ms^{-2}}$)
h_g = geyser eruption height (m)
H = vertical pipe length (m)
$\dot{M}$ = air mass flow rate (kg $\mathrm{s^{-1}}$)
P = pressure (Pa)
R = individual gas constant ($\mathrm{Jkg^{-1}K^{-1}}$)
R = Reynolds number (–)
T = absolute temperature (K)
V = volume ($\mathrm{m^3}$)
We = Weber number (–)
y_o = initial water depth in vertical pipe (m)
α = empirical constant (–)
Δt = duration of geysering event (s)
ν = kinematic viscosity ($\mathrm{m^2\ s^{-1}}$)
ρ = density (kg $\mathrm{m^{-3}}$)
σ = surface tension (N $\mathrm{m^{-1}}$)

Subscripts

a = air
w = water

References

Elperin, T., & Fominykh, A. (1996, Aug 01). Effect of gas release and condensation on characteristics of two-phase gas-and vapor-liquid slug flow. *Heat and Mass Transfer*, *31*(6), 387–391. Retrieved from https://doi.org/10.1007/BF02172584

EPA. (2004). *Impacts and Control of CSOs and SSOs* (Report to Congress No. EPA 833-R-04-001). Office of Water (4203), Washington, D.C. 20460: United States Environmental Protection Agency.

Guo, Q., & Song, C. S. S. (1991). Hydrodynamics under transient conditions. *J. Hydraul. Eng*, *117*(8), 1042-1055.

Hamam, M. A., & McCorquodale, J. A. (1982). Transient conditions in the transition from gravity to surcharged sewer flow. *Can. J. Civ. Eng.*, *9*, 189-196.

Leon, A. S. (2016a). Mathematical models for quantifying eruption velocity in degassing pipes based on exsolution of a single gas and simultaneous exsolution of multiple gases. *J. volcanology and geothermal research*, *323*(1), 72-79.

Leon, A. S. (2016b). New evidence on the causes of explosives geysers in stormwater and combined sewer systems: A simplified model for the prediction of these geysers. In *World environmental and water resources congress 2016.*

Leon, A. S. (2017). Mechanisms that lead to violent geysers in vertical shafts. *Journal of Hydraulic Research (under review).*

Leon, A. S., Ghidaoui, M. S., Schmidt, A. R., & García, M. H. (2010). A robust two-equation model for transient mixed flows. *Journal of Hydraulic Research*, *48*(1), 44-56.

Lewis, J. M. (2011). *A physical investigation of air/water interactions leading to geyser events in rapid filling pipelines* (Unpublished doctoral dissertation). University of Michigan.

Minnesota-DOT. (1999). *7/3/1999 full raw traffic camera catching explosive storm sewer flooding.* Retrieved 2010-10-10, from `http://www.youtube.com/watch?v=4aQySL0sKys`

Pfister, M., & Chanson, H. (2014). Two-phase air-water flows: Scale effects in physical modeling. *Journal of Hydrodynamics, Ser. B*, *26*(2), 291 - 298. Retrieved from `http://www.sciencedirect.com/science/article/pii/S1001605814600329`

Sefko, S., & Edin, B. (2015). Analysis of droplet deposition in a vertical air-water dispersed flow. *Procedia Engineering*, *100*, 105 - 114. Retrieved from `http://www.sciencedirect.com/science/article/pii/S1877705815003756` (25th DAAAM International Symposium on Intelligent Manufacturing and Automation, 2014)

Shao, Z. S. (2013). *Two-dimensional hydrodynamic modeling of two-phase flow for understanding geyser phenomena in urban stormwater system* (Unpublished doctoral dissertation). University of Kentucky, Lexington, KY.

Sharaf, S., der Meulen, G. P. V., Agunlejika, E. O., & Azzopardi, B. J. (2016). Structures in gas–liquid churn flow in a large diameter vertical pipe. *International Journal of Multiphase Flow*, *78*, 88 - 103. Retrieved from `http://www.sciencedirect.com/science/article/pii/S0301932215002037`

Stefanski, S., Kalawa, W., Mirek, K., & Stepien, M. (2017). Visualization and research of gas-liquid two phase flow structures in cylindrical channel. *E3S Web Conf.*, *14*, 01026. Retrieved from `https://doi.org/10.1051/e3sconf/20171401026`

Vasconcelos, J. G. (2005). *Dynamic approach to the description of flow regime transition in stormwater systems* (Unpublished doctoral dissertation). University of Michigan.

Wright, S. J., Lewis, J. W., & Vasconcelos, J. G. (2011). Geysering in rapidly filling storm-water tunnels. *J. Hydraul. Eng*, *137*(1), 112-115.

Zhang, Y., & Kling, G. W. (2006). Dynamics of lake eruptions and possible ocean eruptions. *Annual Review of Earth and Planetary Sciences*, *34*(1), 293-324. Retrieved from `http://dx.doi.org/10.1146/annurev.earth.34.031405.125001`

List of Tables

List of Figures

Table 1 Initial absolute air pressure heads (m) in the upstream tank

Dropshaft length (m)	Initial water vol. = 0.7760 m^3	Initial water vol. = 0.9615 m^3
12	42.2 - 43.6	52.1 - 54.9
9	35.9 - 37.3	45.0 - 47.8
6	30.2 - 31.6	37.3 - 40.1
3	23.9 - 25.3	30.9 - 33.0

Table 2 Mean and coefficient of variation of geyser heights for the non-orifice experiments (non-visualization experiments)

Vertical pipe length (m)	Average geyser height (m)	Coefficient of variation (%)
3	4.3	34.9
6	12.3	27.6
9	23.0	12.6
12	24.9	14.1

Figure 1 Snapshot of a geyser produced in one of the present laboratory experiments. The length of the vertical in this case was 6 m.

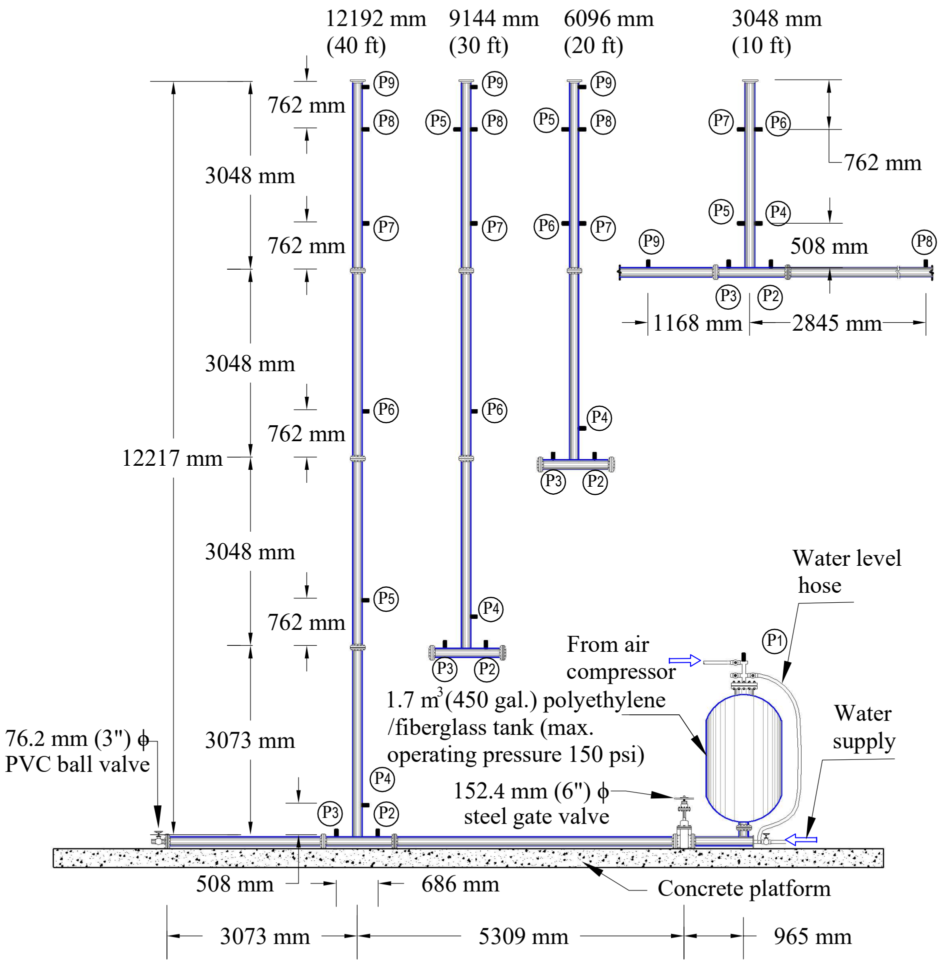

Figure 2 Sketch of experimental setup (Not To Scale), where P1 indicates the location of pressure transducer 1 and so on

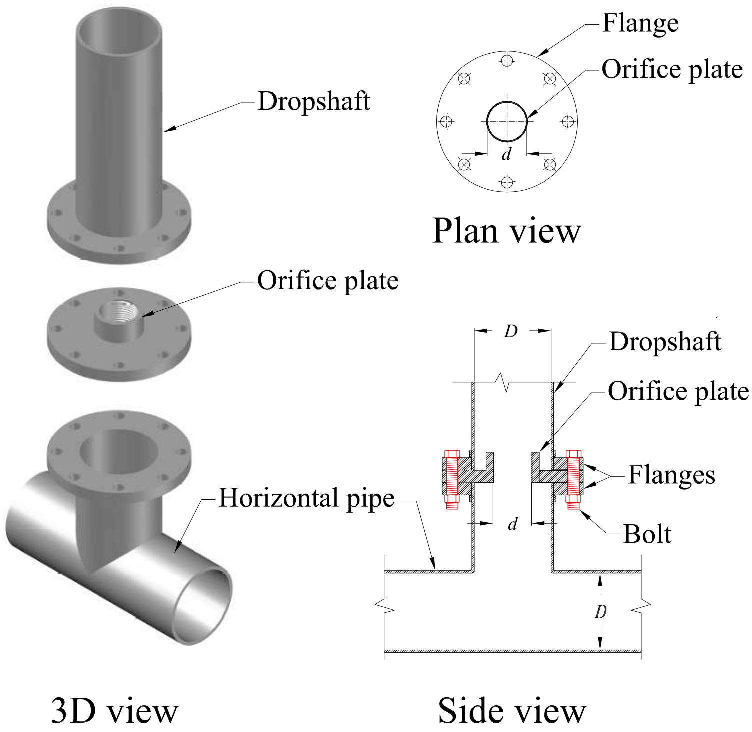

Figure 3 Sketch of orifice installed at bottom of vertical pipe for reducing the air mass flow rate entering the vertical pipe (Not To Scale)

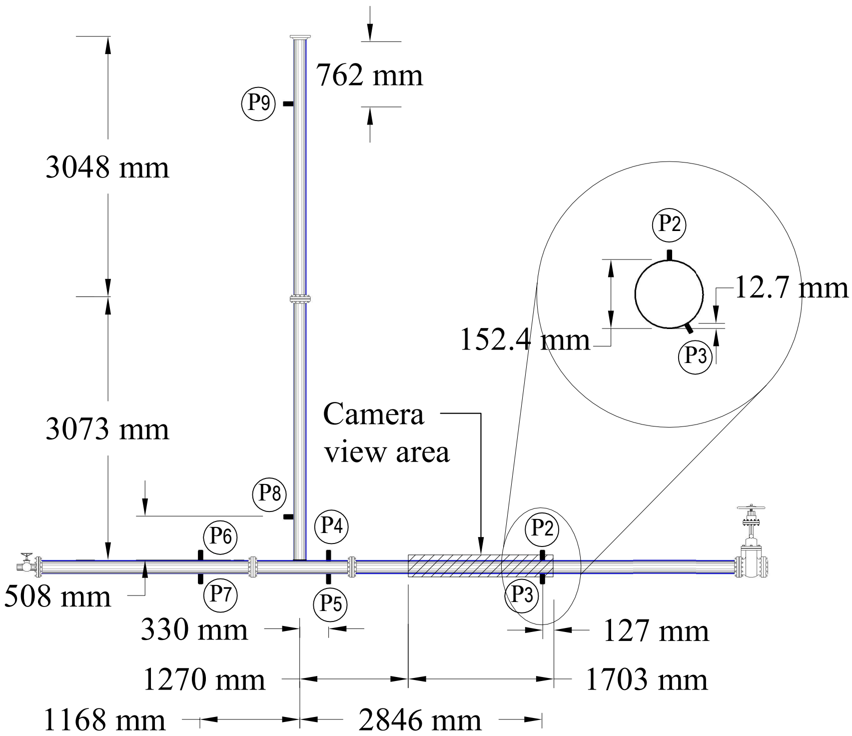

Figure 4 Location of pressure sensors for the visualization experiments (vertical pipe length = 6 m)

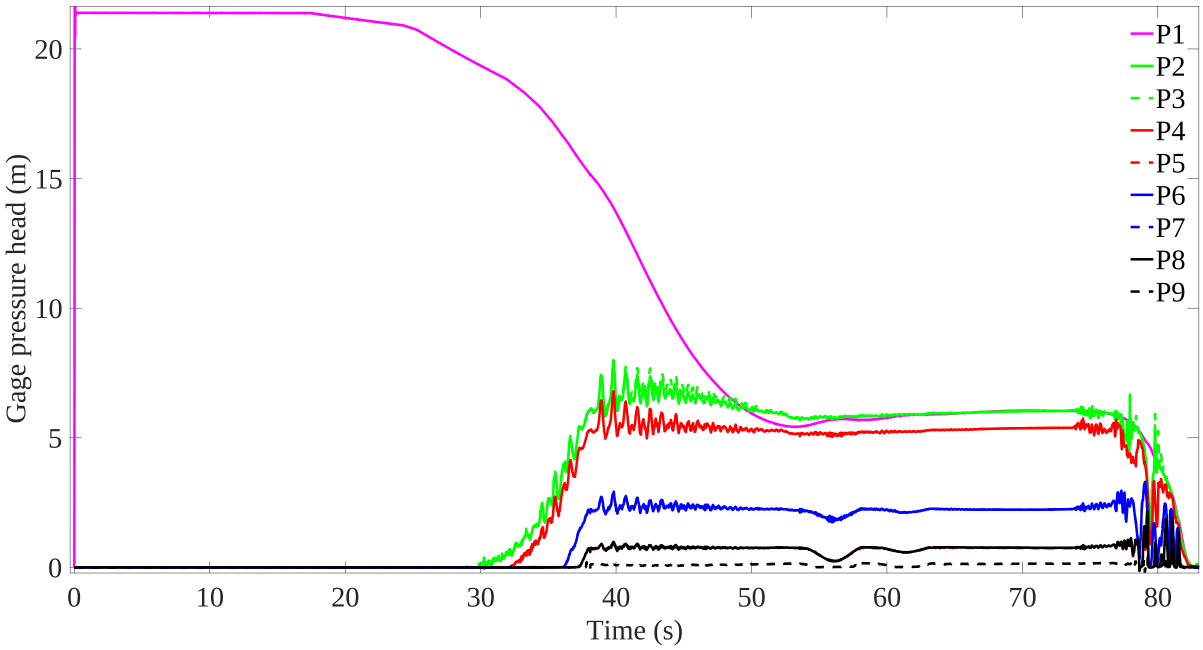

Figure 5 Example of complete time trace of pressure heads recorded for a vertical pipe length of 6 m (Non-visualization experiments).

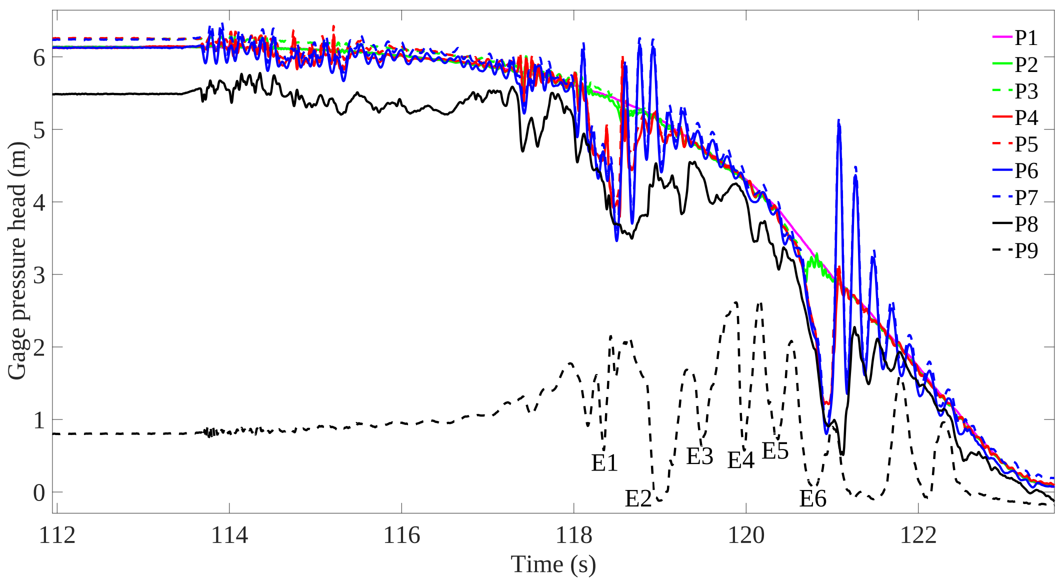

Figure 6 Example of pressure heads for the visualization experiments (vertical pipe length = 6 m)

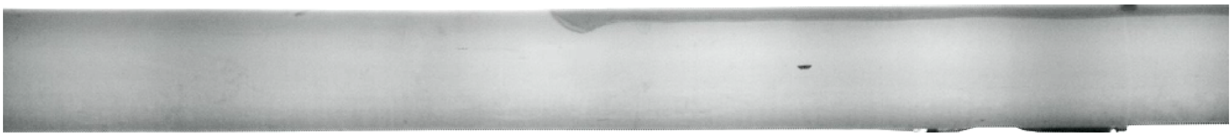

(1) $t = 110.086$ s

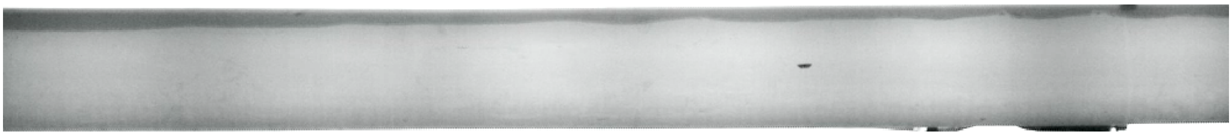

(2) $t = 114.411$ s

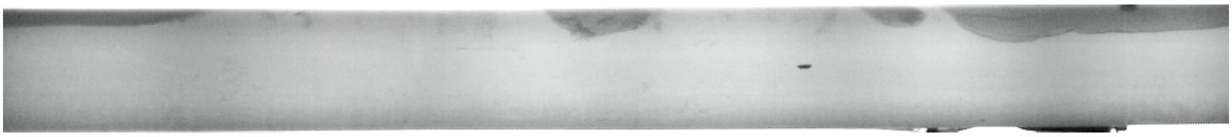

(3) $t = 114.711$ s

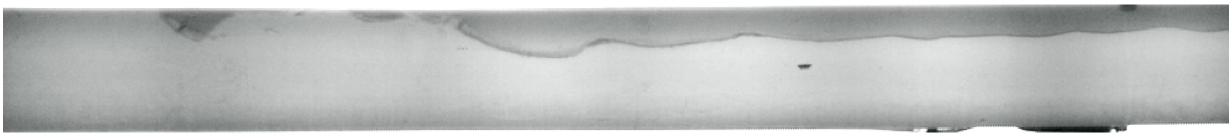

(4) $t = 115.336$ s

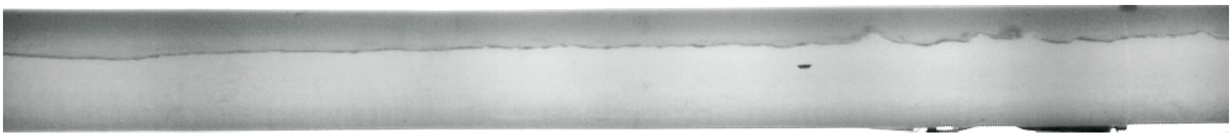

(5) $t = 117.961$ s

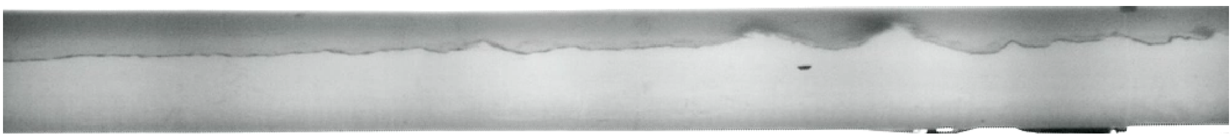

(6) $t = 118.111$ s

Figure 7 Flow snapshots in the horizontal pipe at various times

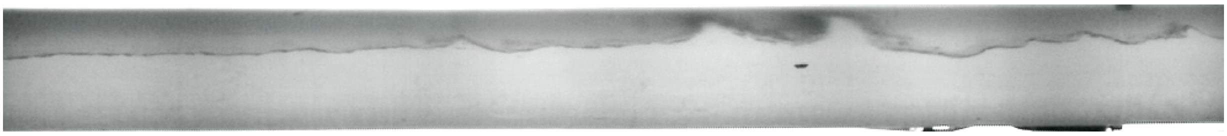

(7) $t = 118.151$ s

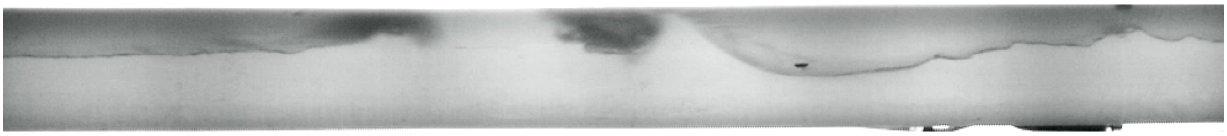

(8) $t = 118.236$ s

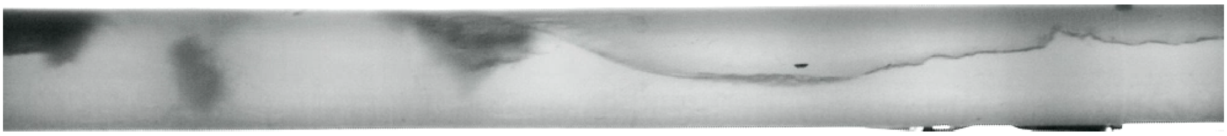

(9) $t = 118.311$ s

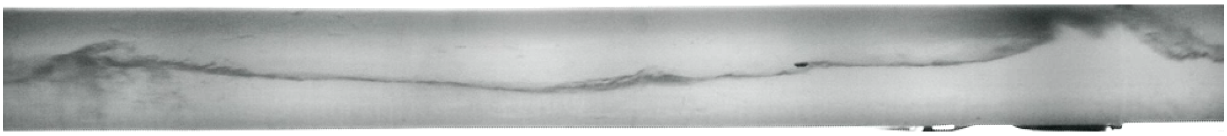

(10) $t = 118.581$ s

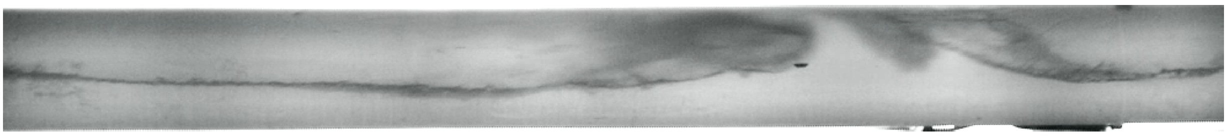

(11) $t = 118.661$ s

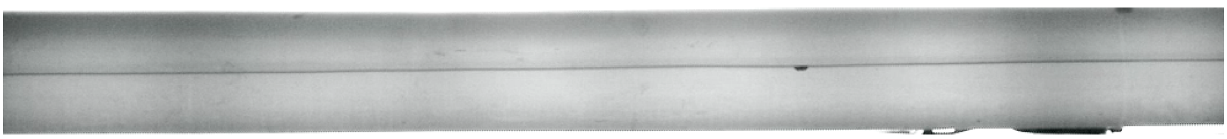

(12) $t = 148.586$ s

Figure 8 *

Flow snapshots in the horizontal pipe at various times (Cont.)

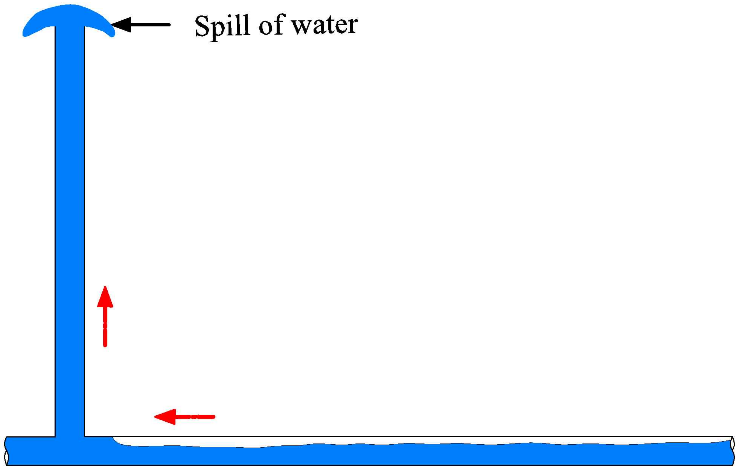

Figure 9 (a) Air pocket approaching vertical pipe

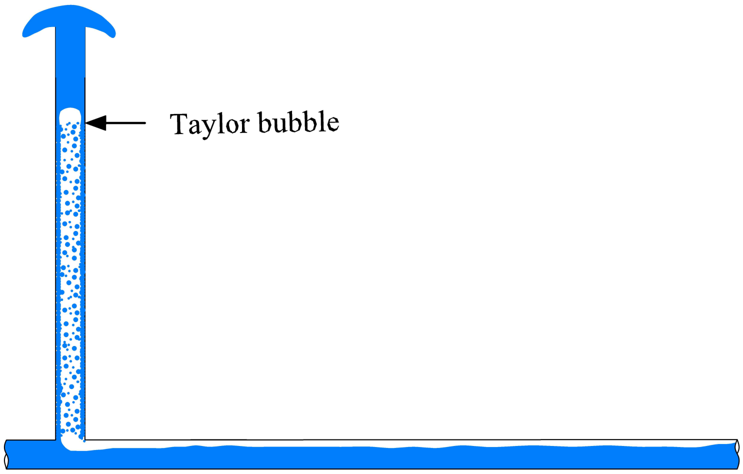

Figure 10 *

(b) Rising of Taylor-like bubble

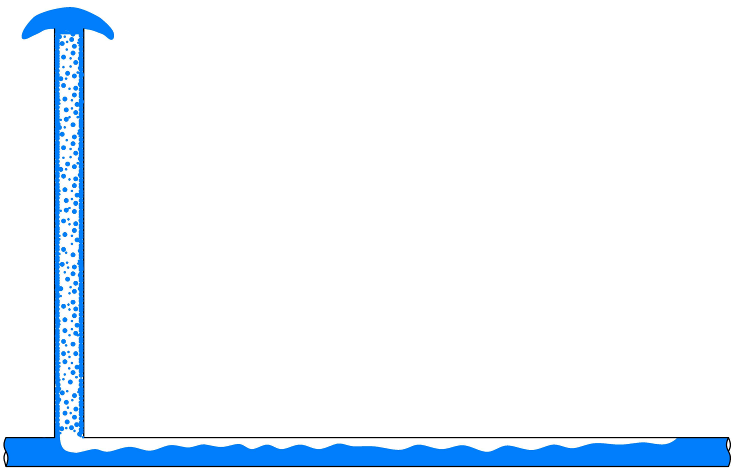

Figure 11 *

(c) Water spill and acceleration of air pocket in horizontal pipe

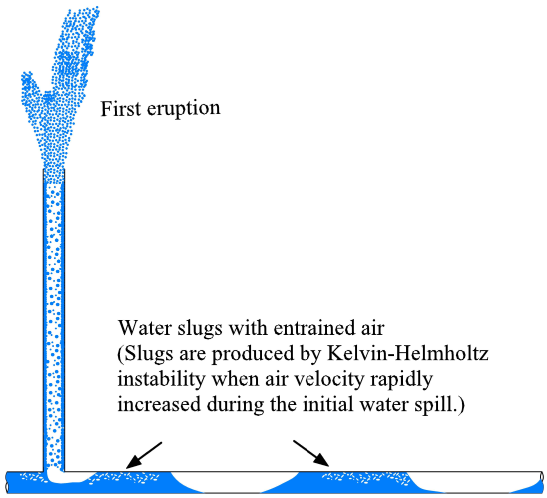

Figure 12 *

(d) First eruption and formation of liquid slugs

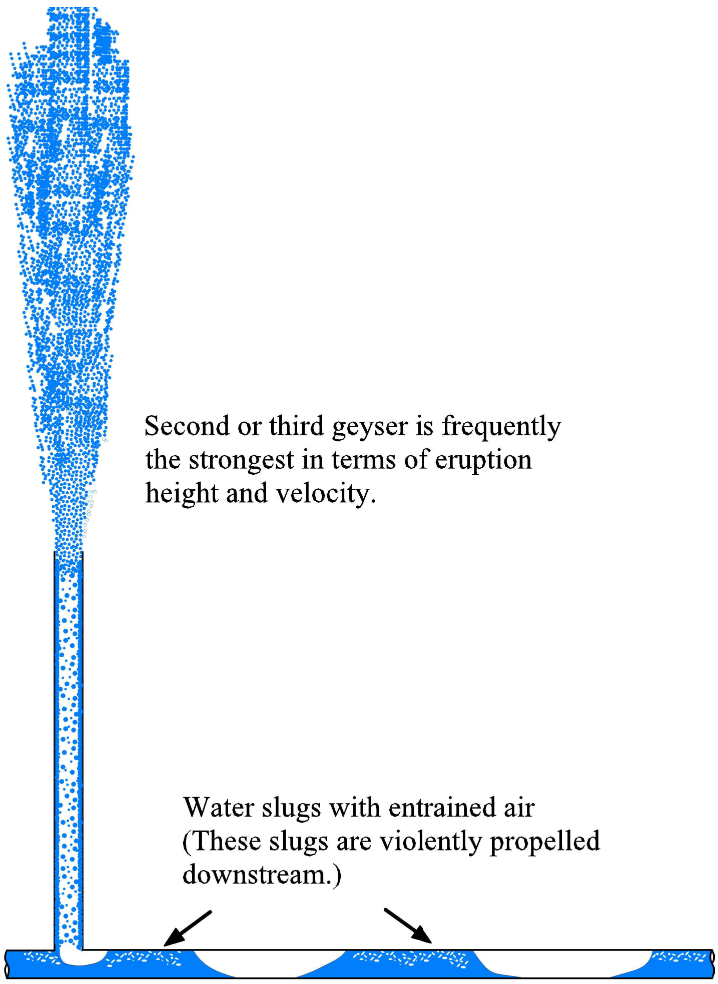

Figure 13 *

(e) Successive eruptions as a result of blowout of slugs

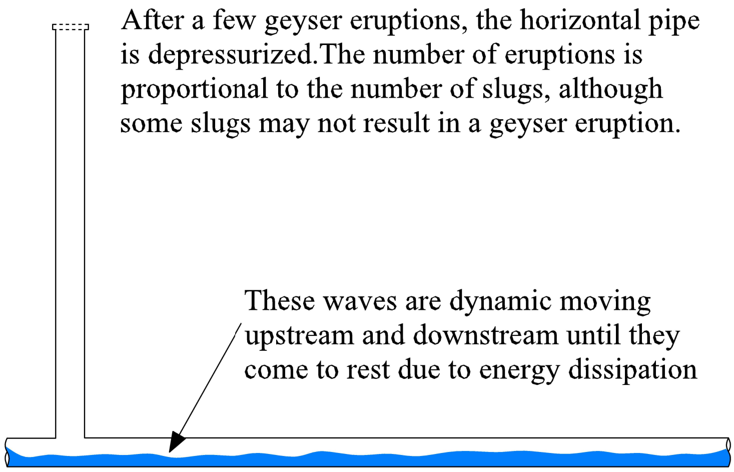

Figure 14 *

(f) Depressurization and propagation of waves in the horizontal pipe

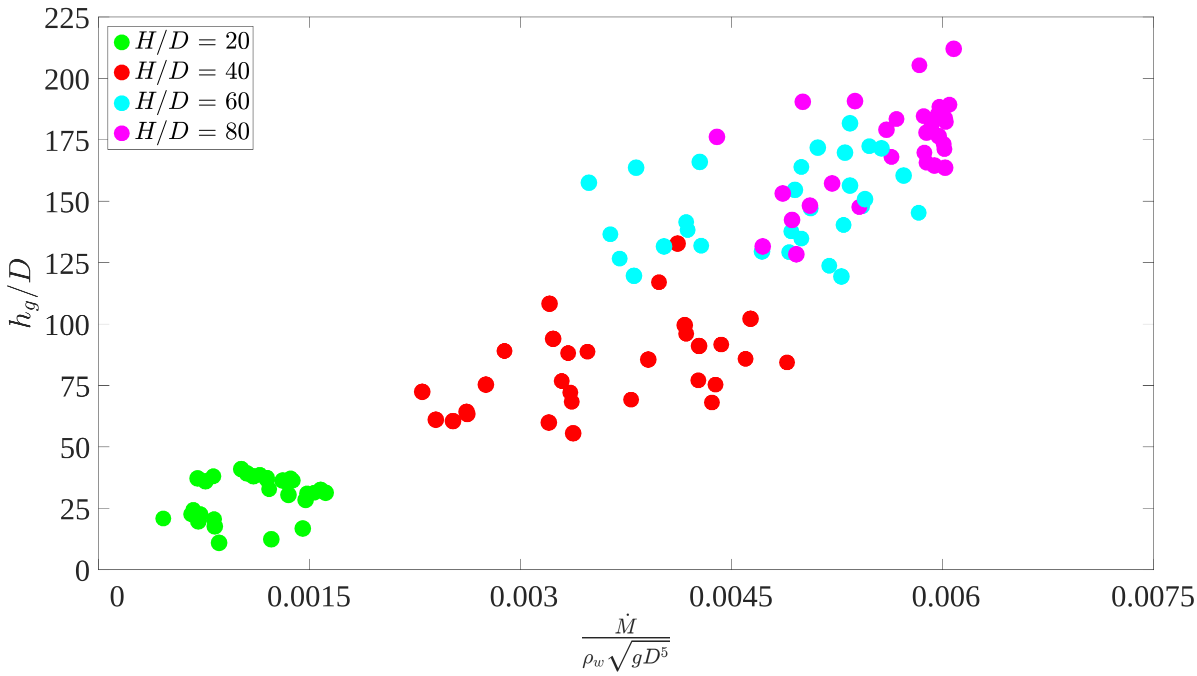

Figure 15 Dimensionless maximum geyser height versus dimensionless air mass flow rate for experiments with no orifice ($y_o = H$, $D_t = D$)

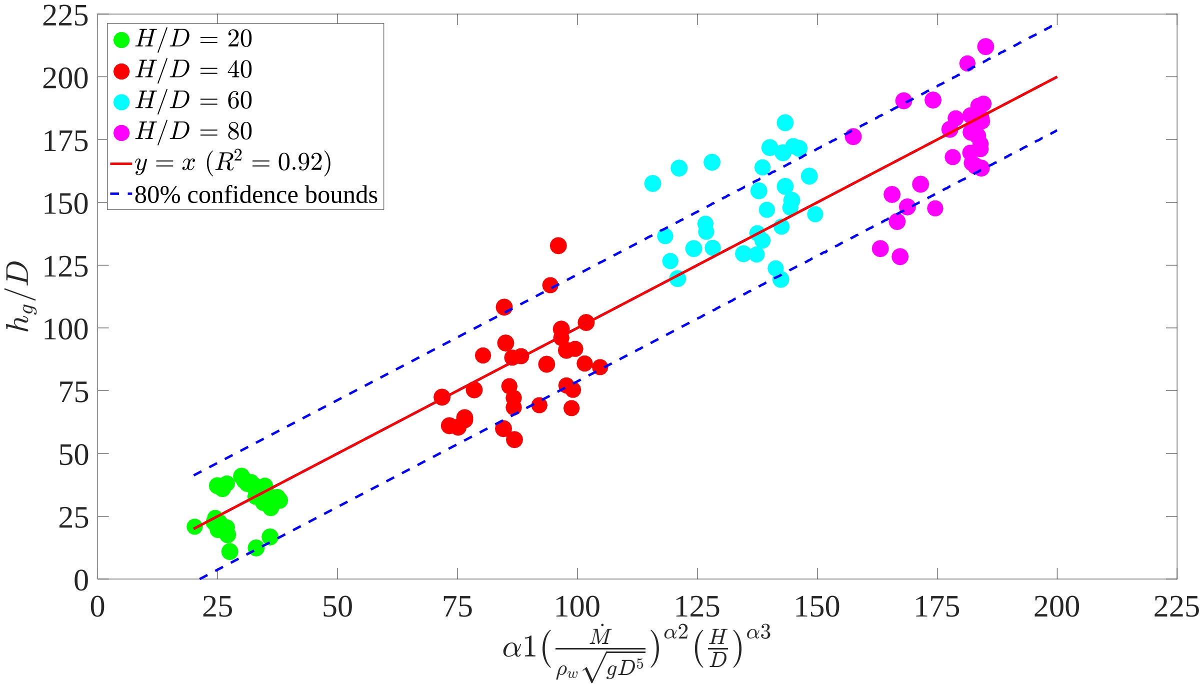

Figure 16 Curve fitting for dimensionless maximum geyser height for experiments with no orifice when $y_o = H$ and $D_t = D$ ($\alpha 1 = 127.887$, $\alpha 2 = 1/2$ and $\alpha 3 = 2/3$)

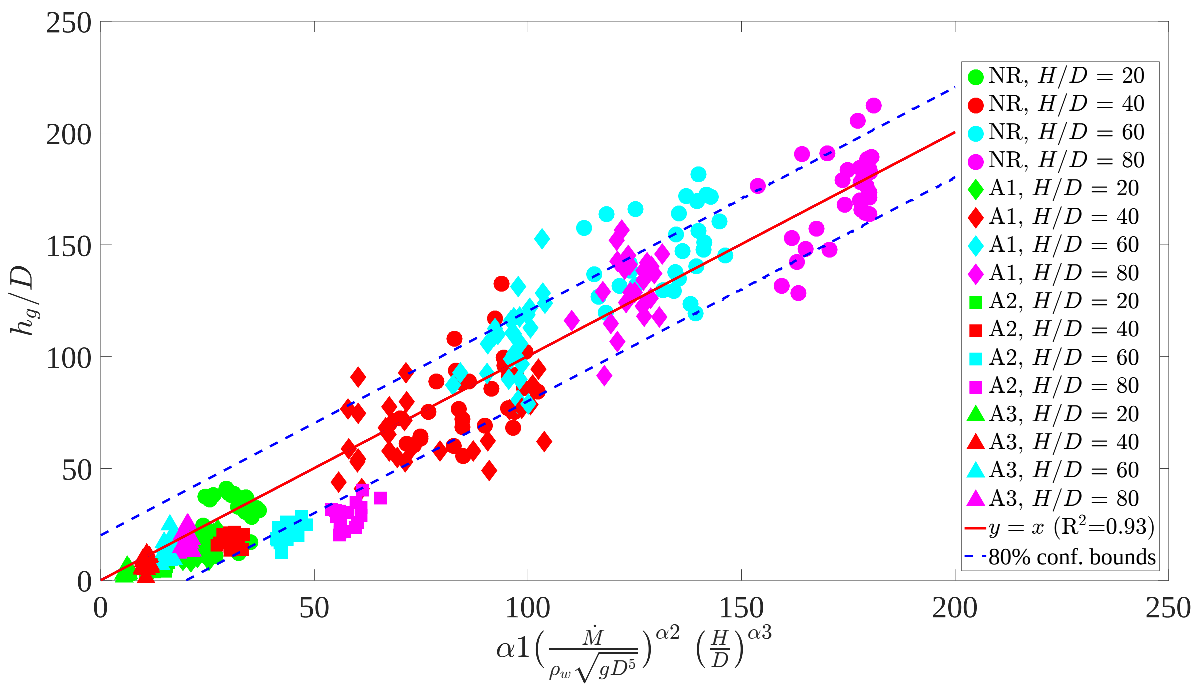

Figure 17 Curve fitting for dimensionless maximum geyser height for orifices A1-A3 and the experiments with no orifice when $y_o = H$ and $D_t = D$ ($\alpha 1 = 124.957$, $\alpha 2 = 1/2$ and $\alpha 3 = 2/3$)